This is the post-print (i.e. final draft post-refereeing) of the publication.
The final publication is available at Wiley Online Library via http://dx.doi.org/ 10.1002/polb.24095

Enhanced Dielectric Performance of a Block Copolymer-Polythiophene Nanocomposite

Maria M. Pérez-Madrigal,[1,2,*] Diego A. Ochoa,[3] Jose E. García,[3] Elaine Armelin[1,2,] and Carlos Alemán[1,2,*]

[1] *Departament d'Enginyeria Química, ETSEIB, Universitat Politècnica de Catalunya, Avda. Diagonal 647, Barcelona E-08028, Spain*

[2] *Center for Research in Nano-Engineering, Universitat Politècnica de Catalunya, Campus Sud, Edifici C', C/Pasqual i Vila s/n, Barcelona E-08028, Spain*

[3] *Departament de Físca, Universitat Politècnica de Catalunya, C/ Jordi Girona 1-3, Barcelona E-08034, Spain*

[*] m.mar.perez@upc.edu and carlos.aleman@upc.edu

ABSTRACT

Dielectric elastomer actuators (DEAs) transform electrical energy into mechanical work. However, despite displaying exceptional features, the low permittivity of elastomers restricts their application. Hence, to overcome this limitation, DEAs are fabricated by dispersing poly(3-methylthiophene acetate) (P3TMA), a polarizable conducting polymer, into poly[styrene-*b*-(ethylene-*co*-butylene)-*b*-styrene] (SEBS), a thermoplastic elastomer with excellent mechanical properties. Although high-quality SEBS:P3TMA films are obtained for all compositions (between 0.5 and 20 wt. % P3TMA), their thickness and surface roughness increase with the nano-sized filler content. Moreover, the conducting particles are well integrated into the SEBS network with no evidence of aggregation or significant change in the mechanical properties of the composites. P3TMA, which forms encapsulated conductive domains within the polymeric matrix, improves the dielectric behaviour of SEBS:P3TMA by increasing their dielectric constant with low dielectric losses and no current leakage. Thus, indicating the potential future application of these nanocomposites as elastomer actuators or high energy density capacitors.

Keywords: dielectric elastomer actuator, polythiophene, polymeric composite, nanoparticles

INTRODUCTION

Electroactive polymers (EAPs) became relevant in the field of soft actuators[1-4] after discovering the piezoelectric response of poly(vinylidene fluoride),[5] which oriented research toward successfully exploring other polymeric materials. Briefly, EAPs respond to electric field stimulation by changing their size or shape (*i.e.* bending, stretching or contracting), thus converting electrical energy into mechanical work. In comparison with electroactive ceramics, EAPs achieve much higher actuation strains (over 300%) with lower power consumption and, also, feature superior resilience properties.[6]

Depending on their actuation mechanism, EAPs can be classified in two groups: ionic EAPs (*e.g.* polymer gels, conducting polymers and carbon nanotubes) and electronic EAPs (*e.g.* ferroelectric polymers, dielectric elastomers, electrostrictive elastomers and liquid crystals elastomers). The actuation response of the former group is based on the diffusion of electrically driven ions, while the latter group involves the movement of surface charges through conductive electrodes patterned on EAPs. Therefore, from a practical point of view, ionic EAPs usually operate in a wet environment, which limits their use, even though there are examples in the literature that report their performance in dry conditions.[7,8]

Within electronic EAPs, dielectric elastomers stand out because of their fast response, large reversible deformation, high energy density, and fatigue resistance.[9] Because of that, they are widely used as actuators (also called dielectric elastomer actuators, DEAs) and sensors,[10] biomimetic systems and robotics,[11] and energy harvesting and storage devices.[12]

There is a great variety of elastomers that have been applied for soft actuation (*e.g.* polyacrylates,[13,14] silicone rubbers,[15-17] polyurethanes[18] and thermoplastic elastomers[19,20]) because of their excellent mechanical and film forming properties, large-scale production and light weight. However, these materials generally tend to display low dielectric constant values (2-10 at 1 kHz).[21] To overcome this drawback, filler particles are dispersed into the elastomeric matrix to increase the overall relative permittivity (ε_r), as well as the actuation strain (*i.e.* ability to store electrical charge). This strategy has successfully been applied using high-permittivity ceramic[22] and metallic fillers,[23,24] carbon black,[25] carbon nanotubes,[26,27] and conducting polymers[28,29] (CPs) such as polythiophene (PTh) and its derivatives.[30,31] Indeed, PTh derivatives have been widely used in organic electronics[32-34] and biomedical applications[35-38] because of their appropriate properties, such as mild polymerization conditions, semiconductor behaviour, and high environmental stability. Furthermore, another method that has been proved to enhance the dielectric permittivity of silicone-based DEA films relies on a binary system of polymeric blends: polydimethylsiloxane-polyethyleneglycol (PDMS-PEG) multiblock copolymer and non-conducting PDMS elastomer.[39]

For instance, Carpi *et al.*[30] showed that the relative dielectric permittivity and the Young's modulus of silicone rubber increases and decreases, respectively, upon blending with a low amount of poly(hexylthiophene) (1-6 wt. %), thus contributing to a remarkable electromechanical response. More recently, Qiao *et al.*[31] reported the synthesis of a methacrylate polymer bearing therthiophene side groups, which behaved as electrically conductive nanoscale domains (< 2 nm). This system exhibited a high dielectric constant and low dielectric losses. Similarly, Huang *et al.*[29] stated that nano-sized fillers enhance the dielectric response.

Nevertheless, within the context of conductive composites, and although high ε_r values are achieved when the filler content approaches the percolation threshold, particle aggregation and blend inhomogeneity lead to poor mechanical integrity (stiffening of the material) and high dielectric losses (Maxwell-Wagner polarization), which reduce considerably the electric breakdown strength of the material. In consequence, strategies such as particle encapsulation,[40,41] chemical grafting,[42,43] or cross-linking of the polymer network[44] have been applied to enhance the compatibility and dispersion of the conductive filler into the host matrix, thus improving the dielectric properties of the polymeric matrix.

The present work develops new DEA films with improved dielectric response by combining poly[styrene-*b*-(ethylene-*co*-butylene)-*b*-styrene] (SEBS) with poly(3-methylthiophene acetate) (P3TMA) nanoparticles. On the one hand, SEBS, a thermoplastic elastomer, has effectively been used as insulating matrix in DEA applications[45,46] due to its adequate mechanical properties (*i.e.* low modulus, high tensile strength and elongation at break) and stretchability.[47] On the other, P3TMA, which is a highly polarizable conducting polymer, is soluble in frequently used organic solvents.[48] Therefore, the high solubility of both materials in chloroform is expected to render a homogeneous and stable blending solution, and thus reduce the impact of P3TMA nanoparticles agglomeration on the mechanical properties of SEBS:P3TMA films. Thus, this facile and straightforward approach (*i.e.* no surfactants or complex procedures required) combined with the fact that conductive fillers improve the dielectric features of insulating polymers[49] represents a successful strategy to fabricate nanocomposites for actuator applications.

Accordingly, SEBS:P3TMA films with increasing content of P3TMA have been prepared and characterized. Special attention has been paid to study the influence of the

P3TMA loading content on the mechanical, dielectric, and electrical properties. Moreover, morphological and topographical observations have been carried out by scanning electron microscopy (SEM) and atomic force microscopy (AFM) to monitor the dispersion of P3TMA into the elastomeric matrix.

METHODS

Materials. 3-Thiophene acetic acid (3TAA) (98.0 %) was purchased from Fluka (Poland). Iron chloride anhydrous (97.0 %), dry methanol (99.5 %) and chloroform ($CHCl_3$) (99.9 %) were purchased from Panreac Quimica S.A.U. (Spain) and used as received, without further purification. A commercially available SEBS resin (Kraton G1650 M) with a 30:70 styrene:rubber ratio was purchased from Kraton. As specified by the provider, this linear triblock copolymer shows the following typical properties: a 300% modulus of 5.5 MPa (ASTM D-412), high tensile strength (34.5 MPa, ASTM D-412), elongation at break of 500 % (ASTM D-412), and good stretchability.

P3TMA synthesis. Poly(3-methylthiophene acetate) (P3TMA, Figure S1a) was prepared by a chemical oxidative coupling polymerization using the procedure described by Kim *et al*.[50] The starting monomer was 3-thiophene methyl acetate (3TMA), which was obtained by refluxing 3TAA in dry methanol for 24 h at 90 ºC, and anhydrous ferric chloride ($FeCl_3$) was used as oxidant and dopant. The purified P3TMA, which was a red-brown powder, was obtained with 61 % yield after removing the residual oxidant and oligomers. P3TMA was fully characterized in our previous works.[51,52] Molecular weights were estimated by size exclusion chromatography (SEC) using 1,1,1,3,3,3-hexafluoroisopropanol as eluent. The number and weight average molecular weights found were Mn = 10,700 g mol^{-1} and Mw = 22500 g mol^{-1}. ^{1}H-NM

(400 MHz, $CDCl_3$) δ = 7.28–7.07 (m, 1H, Ar-H), 3.68 (s, 2H, –CH_2–), 3.63 (s, 3H, O–CH_3); ^{13}C-NMR (100 MHz, $CDCl_3$) δ = 170.8 (C=O), 136–124 (Ar–C), 52.1 (O–CH_3), 34.3 (CH_2).

Preparation of SEBS:P3TMA films. Stock solutions of SEBS (0.13 g mL^{-1}) and P3TMA (1 wt. %) were prepared by using $CHCl_3$ as solvent. P3TMA was submitted to sonication for 10 min before (*i.e.* as powder) and after its dissolution in $CHCl_3$. Finally, the solution was cotton-filtered and stirred for 2 h at room temperature. SEBS was dissolved in $CHCl_3$ by stirring at room temperature until the complete dissolution of the polymer (*ca.* 30 min). SEBS:P3TMA films were obtained with a P3TMA content of 0.5, 1, 2.5, 5, 10 and 20 wt. % (wt. % value refers to the ratio of P3TMA mass to the total mass of the film after complete $CHCl_3$ evaporation). For that, the P3TMA and SEBS solutions were mixed in the appropriate proportion to reach specific compositions. After stirring for 1 h, SEBS:P3TMA mixtures were manually deposited onto glass dishes coated with Teflon®, and subsequently dried at room temperature for 24 h.

Optical and surface characterization. Static Light Scattering (SLS) measures were performed with a Vasco Particle Size Analyzer (Corduan Technology) by using the NanoQ software for data collection and evaluation.

Cross-sections of the films were examined by scanning electron microscopy (SEM) using a Focused Ion Beam Zeiss Neon40 scanning electron microscope equipped with an energy dispersive X-ray (EDX) spectroscopy system and operating at 5 kV. Samples, which were freeze-fractured with liquid nitrogen and mounted vertically onto the support, were sputter-coated with a thin carbon layer of 6-10 nm using a K950X Turbo Evaporator to prevent electron charging problems.

Surface morphology and topography were studied by atomic force microscopy (AFM) using a silicon TAP 150-G probe (Budget Sensors, Bulgaria) with a frequency

of 150 kHz and a force constant of 5 N m^{-1}. Images were obtained in tapping mode with an AFM MultimodeTM (Veeco) using a NanoScope controller under ambient conditions. The Root Mean Square roughness (RMS Rq), which is the average height deviation taken from the mean data plane, was determined using the statistical application of the NanoScope Analysis software.

Mechanical properties. Uniaxial elongation tests on rectangular samples (n = 10) with an area of about 30×3 mm^2 were performed using a Zwick Z2.5/TM1S (Zwick GmbH & Co KG, Germany) machine. Once samples were secured in the frame, tensile testing was conducted at room temperature and samples were strained at a constant deformation speed of 10 mm min^{-1} until breakage. The Young's modulus was determined from the slope in the linear elastic region (*i.e.* below 5 % strain).

Dielectric properties. Both sides of SEBS:P3TMA films with uniform thickness and without defects (bubbles or cracks) were painted with silver paint. After drying at room temperature for 24 hours, films were placed between two copper electrodes, and the complex admittance was measured in the frequency range from 100 Hz to 10 MHz using a precision impedance analyser Agilent 4294A. To ensure reproducibility, six films were tested for each composition (data shown is the mean value). Real (ε_r', dielectric constant) and imaginary (ε_r'', dielectric losses) parts of the relative permittivity were calculated by applying the following expressions:

$$\varepsilon_r' = \frac{B \cdot t}{\varepsilon_0 \cdot 2\pi \cdot f \cdot A} \quad (1)$$

$$\varepsilon_r'' = \frac{G \cdot t}{\varepsilon_0 \cdot 2\pi \cdot f \cdot A} \quad (2)$$

where G and B are the real (conductance) and imaginary (susceptance) parts of the measured admittance, respectively, f is the frequency (Hz), and A and t are the film area

and thickness values, respectively. Finally, the dielectric loss tangent ($\tan\delta$) is expressed as:

$$\tan\delta = \frac{\varepsilon_r''}{\varepsilon_r'} \quad (3)$$

Electrochemical Impedance Spectroscopy (EIS). EIS measurements were performed using an AUTOLAB PGSTAT302N in the 1 MHz – 100 mHz frequency range and sinusoidal voltage amplitude of 10 mV. All experiments were carried out at room temperature. SEBS:P3TMA films of 1.767 cm^2 area were sandwiched between two stainless steel (AISI 316L) electrodes (diameter= 1.5 cm) assembled into an isolating holder.[53] The cell was tightened with screws. However, prior cell closing, samples were immersed in buffered saline solution (PBS, pH = 7.4) at room temperature for 12 h, water excess being wiped out with a tissue. After data collection, the results were processed and evaluated using the Frequency Response Analyser software (FRA software, Eco Chemie B.V, version 4.9.007).

Statistical Analysis. The results obtained from the characterization of the mechanical and dielectric properties are displayed as the mean of at least four replicates ± the standard deviation (Table 1). Besides, ANOVA and Tukey tests were performed to determine the statistical significance of the thickness, RMS roughness (Rq) assessed by AFM, mechanical and dielectric properties. A confidence level of 95% ($p < 0.05$) was considered.

RESULTS AND DISCUSSION

Preparation and characterization of SEBS:P3TMA films

Generally, despite the excellent mechanical properties and processability of elastomers, their technological application as actuators is restricted by their low

dielectric constant. To improve the overall dielectric performance, electrically conductive particles are dispersed into the elastomeric matrix.[23-29] This approach, albeit successful, deteriorates the mechanical integrity of the system if particles aggregate (*i.e.* blend inhomogeneity). Hence, efforts have been focused in improving the surface compatibility between the conductive filler and the host matrix,[40-44] which makes the design process more complex and expensive.

In this work, we have prepared dielectric enhanced polymeric nanocomposites following a straightforward and low-cost blending technique in which poly(3-methylthiophene acetate) (P3TMA) is used as the conductive filler. Specifically, the electron-withdrawing carboxylate groups of P3TMA (Figure S1a) are responsible for its high solubility in chloroform, thus giving rise to a stable blending solution. The size of P3TMA particles in the stock solution (1.0 wt. % $CHCl_3$) was determined to be homogeneous by SLS measurements: the diameter of almost 80 % of P3TMA particles was below 270 nm, while that of the 92 % was under 800 nm. The size of the remaining 8% varied between 0.8 and 1.1 μm.

SEBS:P3TMA films with different compositions (0.5, 1, 2.5, 5, 10 and 20 wt. %) were successfully prepared by solvent casting, and their colour varied from dark yellow to reddish brown depending on the P3TMA content (Figure S1b). Table 1 summarizes the main features for SEBS and SEBS:P3TMA films. For instance, SEBS:P3TMA films, with thickness values varying between 130 ± 33 μm and 220 ± 60 μm, were thicker than SEBS films (94 ± 29 μm). The results from FTIR spectroscopy (Figure S2) evidenced that the components of SEBS:P3TMA films are only mixed physically, with no chemical interaction identified. Figure S2b displays the FTIR spectra of SEBS and P3TMA. Absorption bands observed for P3TMA are in good agreement with those analysed in a previous work,[54] whereas the SEBS spectrum is fully consistent with the

literature available on this tri-block copolymer.[47,55] Further discussion on the assignment of the absorption bands can be found in the Electronic Supporting Information (ESI).

UV-vis spectroscopy measurements of SEBS:P3TMA films (refer to ESI for method and data) evidenced π-π stacking interactions arising from the intramolecular aggregation of P3TMA polymeric chains in films with higher CP concentration. Therefore, the distribution of P3TMA nanoparticles in the SEBS matrix was first examined by SEM (Figure 1). In all the cases, particles are well integrated into the SEBS network, and the surface irregularity increases with the content of P3TMA. This feature is particularly evident for films containing 10 and 20 wt. % P3TMA. Then, AFM measurements were conducted to provide topographical characterization of SEBS:P3TMA films. Figure S4 displays representative AFM topographic height and phase images for SEBS and SEBS:P3TMA surfaces (2.5, 5, 10 and 20 wt. %). The surface roughness increases systematically with the concentration of CP (Figure 2), which is consistent with SEM observations. Specifically, RMS Rq values grew from 59 ± 3 nm for SEBS nm to 178 ± 33 nm for films loaded with 20 wt. % P3TMA, which represents an increment of nearly 200 %. Moreover, AFM phase images for 2.5 and 5 wt. % SEBS:P3TMA films reflect heterogeneity by displaying two different regions. In contrast, phase images for 10 and 20 wt. % SEBS:P3TMA films exhibit lower phase contrast, thus evidencing that samples with such conductive filler loading present higher degree of homogeneity.

Overall, SEBS:P3TMA nanocomposite films are easily prepared with high quality features: flexibility, uniformity and homogeneous morphology. According to this achievement, research was further conducted to evaluate their mechanical, dielectric and interfacial properties.

Mechanical properties

Loaded nanoparticles reduce the flexibility and stretchability of the polymeric matrix they are embedded into.[56] In order to use SEBS:P3TMA films as dielectric elastomer actuators, it is essential to monitor the influence of P3TMA content on their mechanical performance. In this work, mechanical properties were carefully evaluated by means of standard uniaxial tensile tests.

Figure 3a shows representative strain-stress curves for SEBS:P3TMA films with different P3TMA wt. % content, whereas Table 1 contains the resulting mechanical properties (elastic modulus, strain at break and tensile strength). All samples exhibit an elastic response with three different regions: a linear elastic behaviour at low strains, a plateau region with a steady slope, and a hardening stage before the breaking point.

The elastic modulus of 0.5 and 1.0 wt. % SEBS:P3TMA films, 120 ± 10 MPa and 117 ± 15 MPa, respectively, are very similar to that shown by SEBS (114 ± 10 MPa). Although this value increases up to 134 ± 23 MPa for 2.5 wt. % SEBS:P3TMA, only samples loaded with 5, 10 and 20 wt. % of P3TMA behave significantly different from SEBS and 0.5 and 1 wt. % SEBS:P3TMA films. More specifically, the elastic modulus increases to 168 ± 37 MPa, 162 ± 29 MPa and 168 ± 28 MPa for 5, 10 and 20 wt. % SEBS:P3TMA films, respectively. Therefore, the elastic behaviour of SEBS:P3TMA films can be categorized in two groups depending on the P3TMA content.

Interestingly, all SEBS:P3TMA samples display strain at break values higher than that shown by SEBS films (Figure 3b). As it occurred for the elastic modulus, two groups can be distinguished. Films with a P3TMA content ≤ 2.5 wt. % exhibit comparable results (898 ± 67 MPa, 886 ± 78 MPa and 940 ± 12 MPa for 0.5, 1 and 2.5 wt. % respectively) that are significantly different from SEBS, while the rest of the

SEBS:P3TMA films show lower strain at break values, even though higher than that of SEBS (Table 1). Only 10 and 20 wt. % SEBS:P3TMA films show significant difference from 2.5 wt. % SEBS:P3TMA. On the other hand, tensile strength is not significantly different (Table 1): the higher values correspond to films containing 5 and 10 wt. % P3TMA (36 ± 11 MPa and 36 ± 14 MPa, respectively). Therefore, the homogeneous distribution of nanoparticles restricts the motion and deformation of SEBS macromolecular chains in films with a high P3TMA wt. % content. However, slight stiffening arises from the interaction between the elastomeric network and P3TMA when the conductive filler content is low. Hence, regarding the mechanical properties, the percolation threshold is found between 2.5 and 5 wt. % P3TMA.

P3TMA nanoparticles modify the mechanical properties of the SEBS matrix but to a minimal extent. According to these results (Table 1), the optimum P3TMA wt. % content in terms of mechanical behaviour is 2.5 wt. %, which renders films with enhanced elongation at break and without significant increase in the elastic modulus.

Dielectric properties

In addition to adequate mechanical properties, SEBS:P3TMA films are determined to exhibit excellent dielectric performance to fulfil the requirements of actuation performance. However, although elastomers are widely chosen as dielectric materials due to their high breakdown strength, their application is limited by their low dielectric constant. Figure S5a indicates that powder P3TMA displays a dielectric constant ε_r' = 13 with little variation over the frequency range, thus P3TMA particle fillers represented an attractive option for preparing SEBS:P3TMA films with enhanced permittivity.

The dielectric properties of SEBS:P3TMA films containing different wt. % of P3TMA nanoparticles were measured at room temperature. For all films, the dielectric constant remains constant throughout the frequency range, revealing the absence of interfacial polarization (*i.e.* Maxwell-Wagner polarization). Figure 4a shows that ε'_r increased progressively with the P3TMA content. Specifically, at 104 Hz, the ε'_r values for 10 and 20 wt. % SEBS:P3TMA films are 5.1 ± 0.3 and 6.3 ± 0.4, respectively, which are almost two-fold in comparison with pure SEBS (2.9 ± 0.3, Table 1). Concretely, ε'_r values for SEBS and all SEBS:P3TMA films (from 1 to 20 wt. %) are significantly different from P3TMA. For films containing higher P3TMA content, 10 wt. % SEBS:P3TMA films differ from SEBS and 5 wt. % samples, while 20 wt. % SEBS:P3TMA is significantly different from all of the rest compositions. The relatively low ε'_r values obtained for SEBS:P3TMA films is consistent with the lack of interfacial effects and with the favourable compatibility between the two polymeric phases, even at high P3TMA content, which is in good agreement with the morphological and topographical observations.

Dielectric losses are very low for all the tested compositions (Figure 4b). Loss tangent values are constant at low frequencies (up to 10^4 Hz) except for 20 wt. % SEBS:P3TMA. A relaxation process starting at frequencies higher than 1 MHz is detected for pure SEBS. This process is also evident for SEBS:P3TMA films and, although the relaxation strength increases with the P3TMA content, no change in the relaxation time is expected due to the introduction of the filler.[57]

Moreover, P3TMA powder exhibits hyperelectronic polarization, which is characteristic of π-conjugated systems, due to the displacement of charge carriers thus forming a very large dipole through polymeric domains.[58] In this case, the charge

migration is associated with conduction losses that increase the loss tangent at low frequencies (Figure S5b). Consequently, hyperlectronic polarization was also expected at low frequencies for SEBS:P3TMA films with high P3TMA content. Nevertheless, loss tangent values are below 0.04 for all SEBS:P3TMA films regardless the conductive filler content. This result suggests that charge mobility is restricted to the P3TMA domains embedded in the SEBS matrix, which form small dipoles with no current leakage and fast dielectric response. Therefore, electron delocalization through P3TMA π-conjugated chains renders SEBS:P3TMA films with loss tangent values suitable for capacitive applications (< 0.1).

The insulator-to-conductor transition in composites that contain conductive fillers can be understood by the percolation theory, which predicts power-law dependence of the effective conductivity and permittivity in relation to the filler degree of connectivity.[59] In a continuous medium, near the percolation threshold (*i.e.* critical filler concentration), this transition can be identified as an abrupt change in the conductivity, while ε_r' increases continuously below the percolation threshold.[60] The length/diameter aspect ratio of the filler and its orientation strongly affects the percolation threshold. For instance, conductive fillers with high aspect ratio (*e.g.* nanofibers and nanotubes) display low percolation threshold values.[61,62] For our system, ε_r' values are constant over the frequency range for all SEBS:P3TMA films with P3TMA content below 10 wt. %, whereas values for films with 20 wt. % start to slope but with low dielectric losses. Accordingly, the system with a 20 wt. % filler concentration is approaching the percolation threshold, even though the insulator-to-conductor transition has not been reached.[23]

SEBS:P3TMA films consist in enhanced dielectric properties in which P3TMA particles form encapsulated conductive domains within the SEBS polymeric matrix. In spite of the limitations discussed above, SEBS:P3TMA is a suitable composite for obtaining transduction effects due to the fully compatibility between the conductive filler and the host. Although efforts have been recently addressed to obtain all-polymeric percolative compounds as valid dielectric materials for soft actuators,[25,29] blending techniques and composite systems are still feasible alternatives for the fabrication of enhanced nanodielectric polymeric composites because of their simplicity, which brings improved versatility, high filler loadings and reduced production costs.[49,57] In addition to that, if the filler and the matrix are chosen adequately, as in the SEBS:P3TMA system, dielectric properties are similar to those shown by more complex systems (ε_r' values between 9 and 11),[31] while the dielectric losses remain low.

Figure of merit (F_{OM})

According to P. Sommer-Larsen and A. Larsen,[63] the actuation performance of DEA films can be evaluated through a figure of merit (F_{OM}). This single parameter combines the material properties in a universal equation:

$$F_{OM} = \frac{3\varepsilon_r'\varepsilon_0 E_{BD}^2}{Y} \quad (4)$$

Therefore, as discussed by the authors,[63] F_{OM} results in a reference value with a two-fold purpose. First, it assesses that the DEA device fulfils its function, relative to its alternatives; and secondly, it guides the optimization process of the elastomer properties.[39,64]

Unfortunately, in this work, the determination of the E_{BD} values for SEBS and SEBS:P3TMA films was not feasible due to equipment limitations, and thus specific values for F_{OM} calculated with Eq. (4) are not presented. In several works, the E_{BD} of SEBS has been reported to decrease upon the addition of fillers. Consequently, considering that the Young's modulus slightly change with the composition (*i.e.* there are no significant differences up to a P3TMA content of 2.5 wt.%), it remains to be determined if the enhancement in the dielectric permittivity of SEBS:P3TMA films from 2.9 ± 0.2 to 6.3 ± 0.4 compensates a possible decrease in the E_{BD} response of the DEA film due to P3TMA loading.

In an effort to assess that, F_{OM} for SEBS:P3TMA films was determined relative to F_{OM} of SEBS as:

$$\frac{F_{OM}}{F_{OM}^{S}} = \frac{\varepsilon_r' Y^{S}}{\varepsilon_r'^{S} Y} \left(\frac{E_{BD}}{E_{BD}^{S}} \right)^{2} \tag{5}$$

where the superindex ^{S} indicates that those parameters correspond to SEBS films with no P3TMA.

By a simple rearrangement of Eq. (5) (refer to ESI), it can be determined that F_{OM} for SEBS:P3TMA films is greater than F_{OM} of SEBS only when the reduction in E_{BD} upon addition of P3TMA in not higher than a certain value (Table S1 and Figure S7 in ESI). Specifically, SEBS:P3TMA films with 2.5 and 20 wt. % allow for the highest reduction in E_{BD}, that is 14.7% and 19.1%, respectively. Therefore, from a theoretical point of view, the composite film with a P3TMA content of 2.5 wt. % performs best relative to the other compositions investigated, which is in good agreement with the mechanical properties discussion. As an example, Stoyanov *et al.* grafted chemically soft gel-state π-conjugated polyaniline macromolecules to a flexible SEBS-based elastomer.[45] For a conductive filler content of 2 vol%, the permittivity of the system

increased (from 2 to 9 at 1 Hz) with little reduction in the E_{BD} (*i.e.* 14%, from 140 V/μm to 120 V/μm).

In a similar way, Kofod *et al.* reported the F_{OM} values for several polymer/conductive filler composite systems (two of them were composed of SEBS)[46] according to Eq. (6):

$$F_{OM} = \frac{\frac{\varepsilon_r' - \varepsilon_r'^S}{\varepsilon_r'^S}}{\nu} \quad (6)$$

where ν is the filler volume fraction.

If we apply Eq. (6) to our system but relative to the weight fraction of P3TMA present, we observe that the lowest content of filler (1 and 2.5 wt. %) results in the highest permittivity enhancement (Table S1 in ESI).

The actuation performance of DEAs depends on the overall of the material properties; it is the balanced contribution of each one of them - high E_{BD}, low Young's modulus, and relatively high dielectric permittivity - that avoids a diminished performance relative to alternatives. In this work, SEBS:P3TMA composite films feature enhanced dielectric constant with low dielectric losses and no current leakage, thus validating the use of P3TMA as conductive filler to render improved dielectric properties. Undoubtedly, further improvement is required to obtain a DEA commercially competitive. Nevertheless, building on these results, we can address research to overcome the drawbacks displayed by elastomers. For instance, further studies will apply this straightforward and affordable approach to silicone-based DEA and extensive electromechanical actuation tests are to be performed.

Electrochemical impedance spectroscopy

EIS measurements were carried out to characterize the bulk and interfacial properties of SEBS:P3TMA films. For this purpose, appropriated samples of 1.5 cm diameter were prepared and sandwiched between two stainless steel electrodes that were separated by a Teflon® holder. This assembly corresponds to a through-plane conductivity homemade cell configuration that was fully described in a previous work.[53] Samples were immersed in a PBS solution for 12h prior the measurement, and the excess of surface water was removed with blotting paper before each assay. In our system, ions (from the electrolyte solution), the counter-ion (Cl^-) and holes (present along the doped P3TMA polymeric chains) act as charge carriers, establishing electron transport paths through the volume of the sample when an AC potential is applied.

Figure 5 shows the Nyquist and Bode plots obtained for SEBS and SEBS:P3TMA films containing 0.5, 5, 10 and 20 wt. % P3TMA. As it can be seen, the Nyquist spectrum for SEBS film only shows a semicircle in the frequency range from 1 MHz to 100 mHz, which was satisfactorily adjusted to the equivalent electronic circuit (EEC) described as ($CPE_1[R_1CPE_2]$) (Figure S6). Therefore, the high-frequency semicircle is ascribed to the parallel combination of the bulk resistance (R_1) and the capacitance of the polymeric system (CPE_1). The straight line inclined at a constant angle at low frequencies is described as a double-layer capacitance (CPE_2) which accounts for new electrode-electrolyte interfaces created as a consequence of PBS absorption and penetration into small defects present in the film. For all the samples, the fitting quality was judged based on the error percentage associated to each circuit component, showing errors lower than 10 %. Ideal capacitor elements were replaced by constant phase elements (CPE), which describe non-ideal capacitor when the phase angle is different from -90º. The CPE impedance is attributed to the distributed surface reactivity, surface

heterogeneity and roughness, non-uniform current and potential distribution, which in turn are related to the electrode geometry and the electrode porosity.[65]

Nyquist and Bode plots for SEBS:P3TMA samples show more than one semicircle and different capacitive/resistive regions, which is characteristic of systems with several phases. Table 2 summarizes the EEC adjusted to each system. The second resistor/capacitor parallel combination (R_2 and CPE_2) corresponds to the film bulk resistance and double-layer capacitance, respectively. In general, the diameter of the semicircles reduces with increasing content of P3TMA filler, thus indicating lower resistance values (Figures 5a and b). More specifically, the R_1 value decreases two orders of magnitude to when comparing SEBS ($1.80 \cdot 10^7$ Ω cm^2) and 20 wt. % SEBS:P3TMA ($7.6 \cdot 10^5$ Ω cm^2).This trend is also detected in the Bode plot where the overall impedance is lower for the film with 20 wt. % P3TMA content (Figure 5c). Besides, the time constant for SEBS:P3TMA films in the high frequency range shifts towards higher frequencies, which indicates higher conductivity (Table 2). If the mean thickness (t) of each film is taken into account, the conductivity can be calculated through the following equation:

$$\sigma = \frac{t}{R_b} \tag{7}$$

where R_b is the bulk film resistance (R_1 or R_2).

The results indicate that the addition of P3TMA nanoparticles increases the density of potential charge carriers and their mobility through the SEBS network, thus influencing the conductivity. And, although the system behaves as a semi-conductor, the conductivity is still low. Therefore, the percolation threshold has not been reached and the charge migration is localized around the P3TMA conductive domains.

CONCLUSIONS

In summary, we have synthesized a new polymeric composite combining SEBS and P3TMA nanoparticles through a simple and affordable procedure. The SEBS:P3TMA system forms high quality films with uniform and continuous morphology. Loading P3TMA nanoparticles influences the mechanical properties of the SEBS matrix, but to a minimal extent. Within this context, the optimum P3TMA content has been found to be around 2.5 wt. % since the resulting composite shows enhanced elongation at break and no significant increase in the Young's modulus value.

The dielectric characterization of SEBS:P3TMA films revealed that ε_r' increases with the P3TMA content for all frequency range (10^2–10^7 Hz). More specifically, at 104 Hz, the ε_r' values showed by films containing 10 and 20 wt. % of P3TMA (ε_r' = 5.1 and 6.3, respectively) are around two-fold in comparison with the value obtained for pure SEBS films (ε_r' = 2.9). Furthermore, even at high filler contents, dielectric losses are very low. Therefore, the charge mobility is restricted to the P3TMA domains embedded in the SEBS matrix, with no current leakage, which is in good agreement with EIS results. Overall, the results presented in this work indicate that SEBS:P3TMA films are promising candidates to perform as dielectric elastomer actuators or high energy density capacitors. Thus, extensive electromechanical actuation tests are to be performed.

ACKNOWLEDGEMENTS

Financial support from the MICINN and FEDER (MAT2012-34498) is gratefully acknowledged. M. M. P.- M. thanks the financial support through a FPI-UPC grant. D.A.O. and J.E.G. acknowledge support from the MINECO (Spanish Government)

project MAT2013-48009-C4-P-2. We also thank Dr. Carlos Díaz Blanco from GBMI (Molecular and Industrial Biotechnology Group, UPC) for technical support during SLS measurements.

REFERENCES

1. Y. Bar-Cohen, T. Xue, B. Joffe, S.-S. Lih, M. Shahinpoor, J. S. Harrison, J. G. Smith, P. Willis, In Proc. SPIE 3041, Conference Proceedings of Smart Structures and Materials: Smart Structures and Integrated Systems, June 6, 1997; Regelbrugge, M. E., Ed.; San Diego, CA, 1997.

2. M. Shahinpoor, Y. Bar-Cohen, J. O. Simpson, J. Smith, *Smart Mater. Struct.* **1998**, *7*, R15.

3. Q. M. Zhang, V. Bharti, X. Zhao, *Science* **1998**, *280*, 2101–2104.

4. Q. M. Zhang, H. Li, M. Poh, F. Xia, Z.-Y. Cheng, H. Xu, C. Huang, *Nature* **2002**, *419*, 284–287.

5. H. Kawai, *Jpn. J. Appl. Phys.* **1969**, *8*, 975–976.

6. Y. Bar-Cohen, In Electroactive polymer (EAP) actuators as artificial muscles: reality, potential, and challenges (2nd Edition); Bar-Cohen, Y., Ed.; SPIE Press: Bellingham, 2004.

7. C. Chevrot, D. Teyssié, F. Vidal, F. Tran-Van, *Materiaux et Techniques* **2009**, *97*, 51-57.

8. G. T. M. Nguyen, A. L. Michan, A. Fannir, M. Viallon, C. Vancaeyzeele, C. A. Michal, F. Vidal, *Eur. Polym. J.* **2013**, *49*, 4108-4117.

9. R. Pelrine, R. Kornbluh, In Dielectric elastomers as electromechanical transducers: fundamentals, materials, devices, models and applications of an emerging electroactive

polymer technology; Carpi, F.; De Rossi, D.; Kornbluh, R.; Pelrine, R.; Sommer-Larsen, P., Eds.; Elsevier: Amsterdam-Boston, 2008; Section I, Chapter 1, pp 3-12.

10. P. Brochu, Q. Pei, *Macromol. Rapid Commun.* **2010**, *31*, 10–36.

11. P. Maiolino, M. Maggiali, G. Cannata, G. Metta, L. Natale, *IEEE Sens. J.* **2013**, *13*, 3910–3917.

12. D. L. Henann, S. A. Chester, K. Bertoldi, *J. Mech. Phys. Solids* **2013**, *61*, 2047–2066.

13. H. Zhang, L. Düring, G. Kovacs, W. Yuan, X. Niu, Q. Pei, *Polym. Int.* **2010**, *59*, 384–390.

14. J. Qiang, H. Chen, B. Li, *Smart Mater. Struct.* **2012**, *21*, 025006.

15. S. Michel, X. Q. Zhang, M. Wissler, C. Löwe, G. A. Kovacs, *Polym. Int*. **2010**, *59*, 391–399.

16. H. Zhao, D.-R. Wang, J.-W. Zha, J. Zhao, Z.-M. Dang, *J. Mater. Chem. A* **2013**, *1*, 3140–3145.

17. F. B. Madsen, A. E. Daugaard, S. Hvilsted, A. L. Skov, *Macromol. Rapid Commun.* **2016**, *37*, 378-413.

18. N.-J. Jo, D.-H. Lim, G.-M. Bark, H.-H. Chun, I.-W. Lee, H. Park, *J. Mater. Sci. Technol.* **2010**, *26*, 763–768.

19. R. Shankar, T. K. Ghosh, R. J. Spontak, *Macromol. Rapid Commun.* **2007**, *28*, 1142–1147.

20. D. Yang, M. Tian, H. Kang, Y. Dong, H. Liu, Y. Yu, L. Zhang, *Mater. Lett.* **2012**, *76*, 229–232.

21. J.-D. Nam, H. R. Choi, J. C. Koo, Y. K. Lee, K.J. Kim, In Electroactive Polymers for Robotics – Artificial Muscles and Sensors; Kim, K. J.; Tadokoro, S., Eds.; Springer-Verlag: London, 2007; Table 2.1., Chapter 2, p 40.

22. G. Gallone, F. Carpi, D. De Rossi, G. Levita, A. Marchetti, *Mater. Sci. Eng. C* **2007**, *27*, 110–116.

23. J. Xu, C. P. Wong, *Appl. Phys. Lett.* **2005**, *87*, 082907.

24. W. Hu, S. N. Zhang, X. Niu, C. Liu, Q. Pei, *J. Mater. Chem. C* **2014**, *2*, 1658–1666.

25. H. Stoyanov, D. McCarthy, M. Kollosche, G. Kofod, *Appl. Phys. Lett.* **2009**, *94*, 232905.

26. Z.-M. Dang, L. Wang, Y. Yin, Q. Zhang, Q. Q. Lei, *Adv. Mater.* **2007**, *19*, 852–857.

27. J.-K. Yuan, S.-H. Yao, A. Sylvestre, J. Bai, *J. Phys. Chem. C* **2012**, *116*, 2051–2058.

28. C. Huang, Q. Zhang, *Adv. Funct. Mater.* **2004**, *14*, 501–506.

29. C. Huang, Q. M. Zhang, J. Su, *Appl. Phys. Lett.* **2003**, *82*, 3502–3504.

30. F. Carpi, G. Gallone, F. Galantini, D. De Rossi, *Adv. Funct. Mater.* **2008**, *18*, 235–241.

31. Y. Qiao, Md. S. Islam, K. Han, E. Leonhardt, J. Zhang, Q. Wang, H. J. Ploehn, C. Tang, *Adv. Funct. Mater.* **2013**, *23*, 5638–5646.

32. D. Aradilla, F. Estrany, C. Alemán, *J. Phys. Chem. C* **2011**, *115*, 8430-8438.

33. D. Aradilla, F. Estrany, F. Casellas, J. I. Iribarren, C. Alemán, *Org. Electr.* **2014**, *15*, 40–46.

34. Y. Wang, S. Tao, Y. An, S. Wu, C. Meng, *J. Mater. Chem. A* **2013**, *1*, 8876–8887.

35. M. Sharma, D. Svirskis, S. Garg, In Smart Materials for Drug Delivery; Alvarez-Lorenzo, C.; Concheiro, A.; Eds.; RSC: London, 2013; Vol. 1, pp 283–303.

36. M. Asplund, T. Nyberg, O. Inganäs, *Polym. Chem.* **2010**, *1*, 1374–1391.

37. A.-D. Bendrea, L. Cianga, I. Cianga, *J. Biomater. Appl.* **2011**, 26, 3–84.

38. M. M. Pérez-Madrigal, E. Armelin, J. Puiggalí, C. Alemán, *J. Mater. Chem. B* **2015**, *3*, 5904–5932.

39. A. H. A. Razak, P. Szabo, A. L. Skov, *RSC Adv.* **2015**, *5*, 53054–53062.

40. M. Molberg, D. Crespy, P. Rupper, F. Nüesch, J.-A. E. Månson, C. Löwe, D. M. Opris, *Adv. Funct. Mater.* **2010**, *20*, 3280–-3291.

41. D. M. Opris, M. Molberg, C. Walder, Y. S. Ko, B. Fischer, F. A. Nüesch, *Adv. Funct. Mater.* **2011**, *21*, 3531–3539.

42. S. Liang, J. Claude, K. Xu, Q. Wang, *Macromolecules* **2008**, *41*, 6265–6268.

43. C. G. Hardy, Md. S. Islam, D. Gonzalez-Delozier, H. J. Ploehn, C. Tang, *Macromol. Rapid Commun.* **2012**, *33*, 791–797.

44. S. S. Hassouneh, A. E. Daugaard, A. L. Skov, *Macromol. Mater. Eng.* **2015**, *300*, 542–550.

45. H. Stoyanov, M. Kollosche, D. N. McCarthy, G. Kofod, *J. Mater. Chem.* **2010**, *20*, 7558–7564.

46. G. Kofod, S. Risse, H. Stoyanov, D. N. McCarthy, S. Sokolov, R. Kraehnert, *ACS Nano* **2011**, *5*, 1623–1629.

47. F. Müller, C. A. Ferreira, L. Franco, J. Puiggalí, C. Alemán, E. Armelin, *J. Phys. Chem. B* **2012**, *116*, 11767–11779.

48. A. L. Gomes, J. Casanovas, O. Bertran, J. S. de C. Campos, E. Armelin, C. Alemán, *J. Polym. Res.* **2011**, *18*, 1509–1517.

49. P. Hu, Y. Shen, Y. Guan, X. Zhang, Y. Lin, Q. Zhang, C.-W. Nan, *Adv. Funct. Mater.* **2014**, *24*, 3172–3178.

50. B. Kim, L. Chen, J. Gong, Y. Osada, *Macromolecules* **1999**, *32*, 3964–3969.

51. E. Llorens, M. M. Pérez-Madrigal, E. Armelin, L. J. del Valle, J. Puiggalí, C. Alemán, *RSC Adv.* **2014**, *4*, 15245–15255.

52. M. Planellas, M. M. Pérez-Madrigal, L. J. del Valle, S. Kobauri, R. Katsarava, C. Alemán, J. Puiggalí, *Polym. Chem.* **2015**, *6*, 925–937.

53. F. Müller, C. A. Ferreira, D. S. Azambuja, C. Alemán, E. Armelin, *J. Phys. Chem. B* **2014**, *118*, 1102–1112.

54. M. M. Pérez-Madrigal, E. Armelin, L. J. del Valle, F. Estrany, C. Alemán, *Polym Chem.* **2012**, *3*, 979–991.

55. T. Zhou, A. Zhang, C. Zhao, H. Liang, Z. Wu, J. Xia, *Macromolecules* **2007**, *40*, 9009–9017.

56. H. Stoyanov, M. Kollosche, S. Risse, D. N. McCarthy, G. Kofod, *Soft Matter* **2011**, *7*, 194–202.

57. G. Gallone, F. Galantini, F. Carpi, *Polym. Int.* **2010**, *59*, 400–406.

58. R. D. Hartman, H. A. Pohl, *J. Polym. Sci., Part A: Polym. Chem.* **1968**, *6*, 1135–1152.

59. D. Stauffer, A. Aharony, In Introduction to percolation theory; Taylor & Francis: London, 1994.

60. S. Kirkpatrick, *Rev. Mod. Phys.* **1973**, *45*, 574–588.

61. A. Celzard, E. McRae, C. Deleuze, M. Dufort, G. Furdin, J. F. Marêché, *Phys. Rev. B* **1996**, *53*, 6209–6214.

62. E. J. Garboczi, K. A. Snyder, J. F. Douglas, M. F. Thorpe, *Phys. Rev. E* **1995**, *52*, 819–828.

63. P. Sommer-Larsen, A. L. Larsen, In Proc. SPIE 5385, Conference Proceedings of Smart Structures and Materials 2004: Electroactive Polymer Actuators and Devices (EAPAD) 68, July 27, 2004; Bar-Cohen, Y., Ed.; San Diego, CA, 2004.

64. L. Yu, F. B. Madsen, S. Hvilsted, A. L. Skov, *RSC Adv.* **2015**, *5*, 49739–49747.

65. J.-B. Jorcin, M. E. Orazem, N. Pébère, B. Tribollet, *Electrochim. Acta* **2006**, *51*, 1473–1479.

This is the post-print (i.e. final draft post-refereeing) of the publication.
The final publication is available at Wiley Online Library via http://dx.doi.org/10.1002/polb.24095

Table 1. SEBS and SEBS:P3TMA film properties: thickness (the value observed by SEM is displayed in parenthesis), RMS roughness (RMS Rq) assessed by AFM, and mechanical and dielectric properties. (-) indicates features not determined for P3TMA (powder).

		Thickness (μm)	RMS Rq (nm)	Elastic Modulus (MPa)	Strain at Break (%)	Tensile Strength (MPa)	ε_r' at 104 Hz
	SEBS	94 ± 29 (125)	59 ± 3	114 ± 10	750 ± 39	25 ± 7	2.9 ± 0.2
SEBS:P3TMA	0.5 wt. %	194 ± 50 (244)	77 ± 1	120 ± 10	898 ± 67	25 ± 6	-
	1 wt. %	130 ± 33 (212)	99 ± 18	117 ± 15	886 ± 78	20 ± 9	3.6 ± 0.6
	2.5 wt. %	220 ± 60 (185)	104 ± 15	134 ± 23	940 ± 12	29 ± 7	4.2 ± 1.0
	5 wt. %	123 ± 42 (163)	103 ± 17	168 ± 37	812 ± 64	36 ± 11	3.8 ± 0.8
	10 wt. %	152 ± 25 (207)	130 ± 32	162 ± 29	794 ± 69	36 ± 14	5.1 ± 0.3
	20 wt. %	167 ± 52 (192)	178 ± 33	168 ± 28	807 ± 77	25 ± 8	6.3 ± 0.4
	P3TMA	-	-	-	-	-	13.1 ± 1.4

Table 2. Equivalent electric circuit (EEC), bulk resistance and conductivity data calculated by EIS for SEBS and SEBS:P3TMA films containing 0.5, 5, 10 and 20 wt. % P3TMA nanoparticles.

		Thickness (μm)	EEC[a]	R_1 (Ω cm^2)	σ_1 (S cm^{-1})	R_2 (Ω cm^2)	σ_2 (S cm^{-1})
	SEBS	171.1	$(CPE_1[R_1CPE_2])$	$1.80\cdot10^{7}$	$9.52\cdot10^{-10}$	-	-
SEBS:P3TMA	0.5 wt.%	120.4	$(CPE_1[R_1(CPE_2R_2)])$	$5.07\cdot10^{6}$	$2.02\cdot10^{-9}$	$8.20\cdot10^{7}$	$1.25\cdot10^{-10}$
	5 wt.%	180.0	$(CPE_1[R_1(CPE_2R_2)])$	$4.01\cdot10^{6}$	$4.49\cdot10^{-9}$	$4.68\cdot10^{6}$	$3.85\cdot10^{-9}$
	10 wt.%	156.0	$(CPE_1R_1)(CPE_2R_2)$	$2.05\cdot10^{6}$	$7.61\cdot10^{-9}$	$5.27\cdot10^{6}$	$2.96\cdot10^{-9}$
	20 wt.%	134.2	$(CPE_1R_1)(CPE_2R_2)$	$7.61\cdot10^{5}$	$1.76\cdot10^{-8}$	$1.06\cdot10^{7}$	$1.27\cdot10^{-9}$

[a] See Figure S6

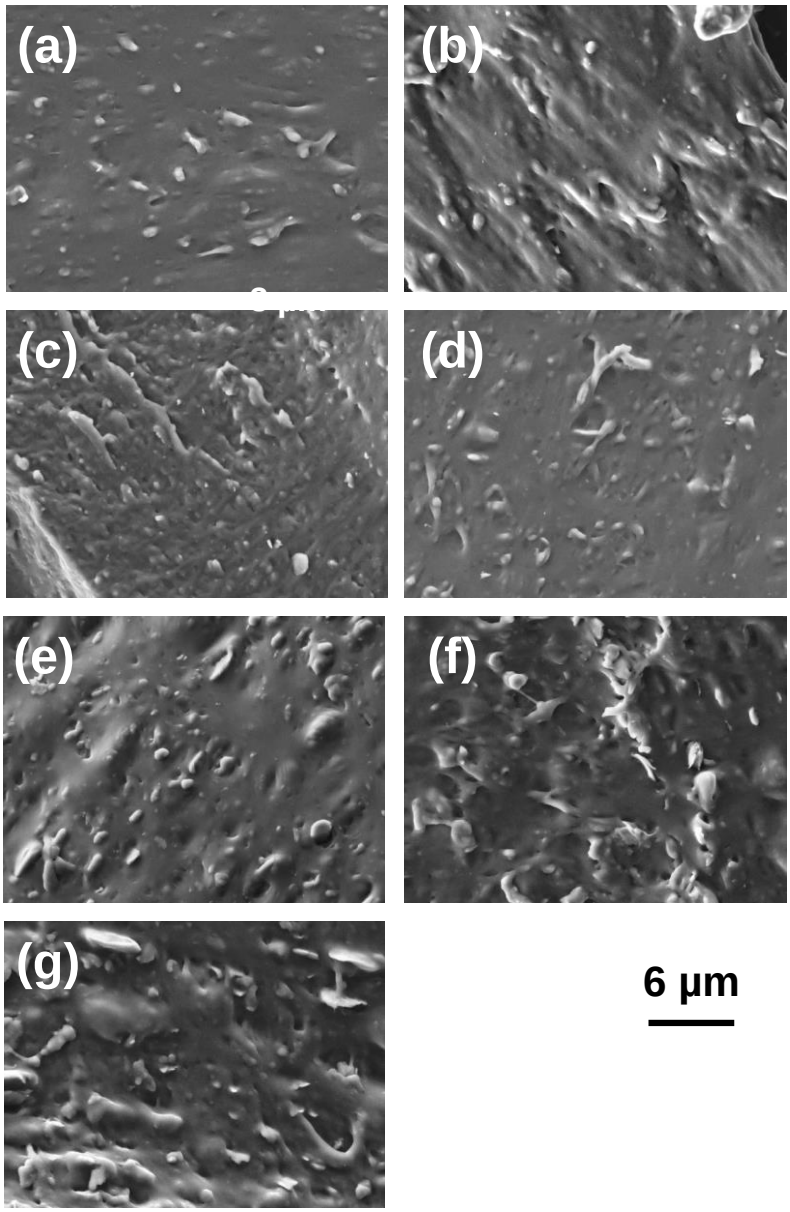

Figure 1. SEM images for (a) SEBS and (b-g) SEBS:P3TMA film cross-sections with increasing P3TMA content: (b) 0.5 wt. %; (c) 1 wt. %; (d) 2.5 wt. %; (e) 5 wt. %; (f) 10 wt. %; and (g) 20 wt. %.

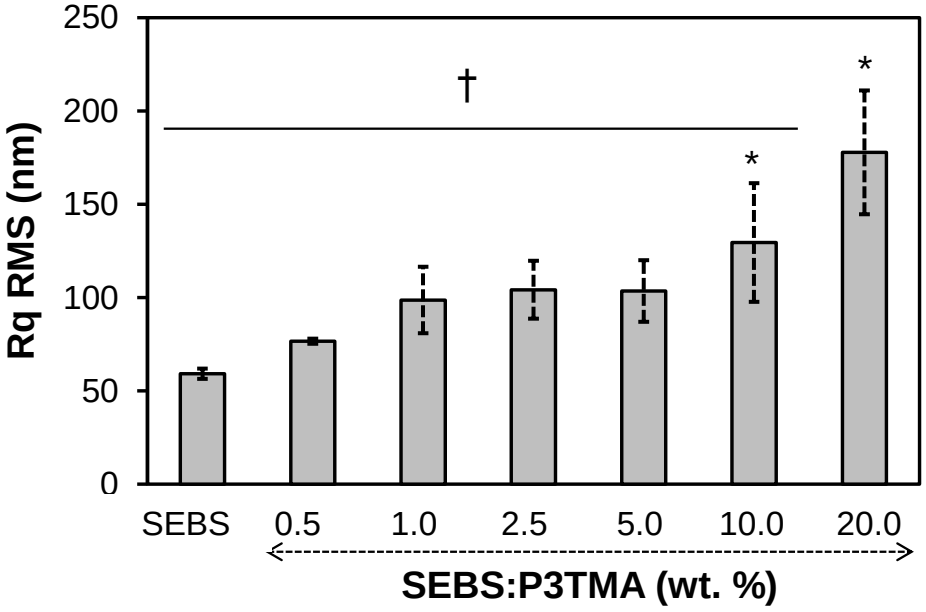

Figure 2. Rq RMS values for SEBS:P3TMA films. Tukey test ($p < 0.05$) * *vs.* SEBS and † *vs.* 20 wt. % SEBS:P3TMA.

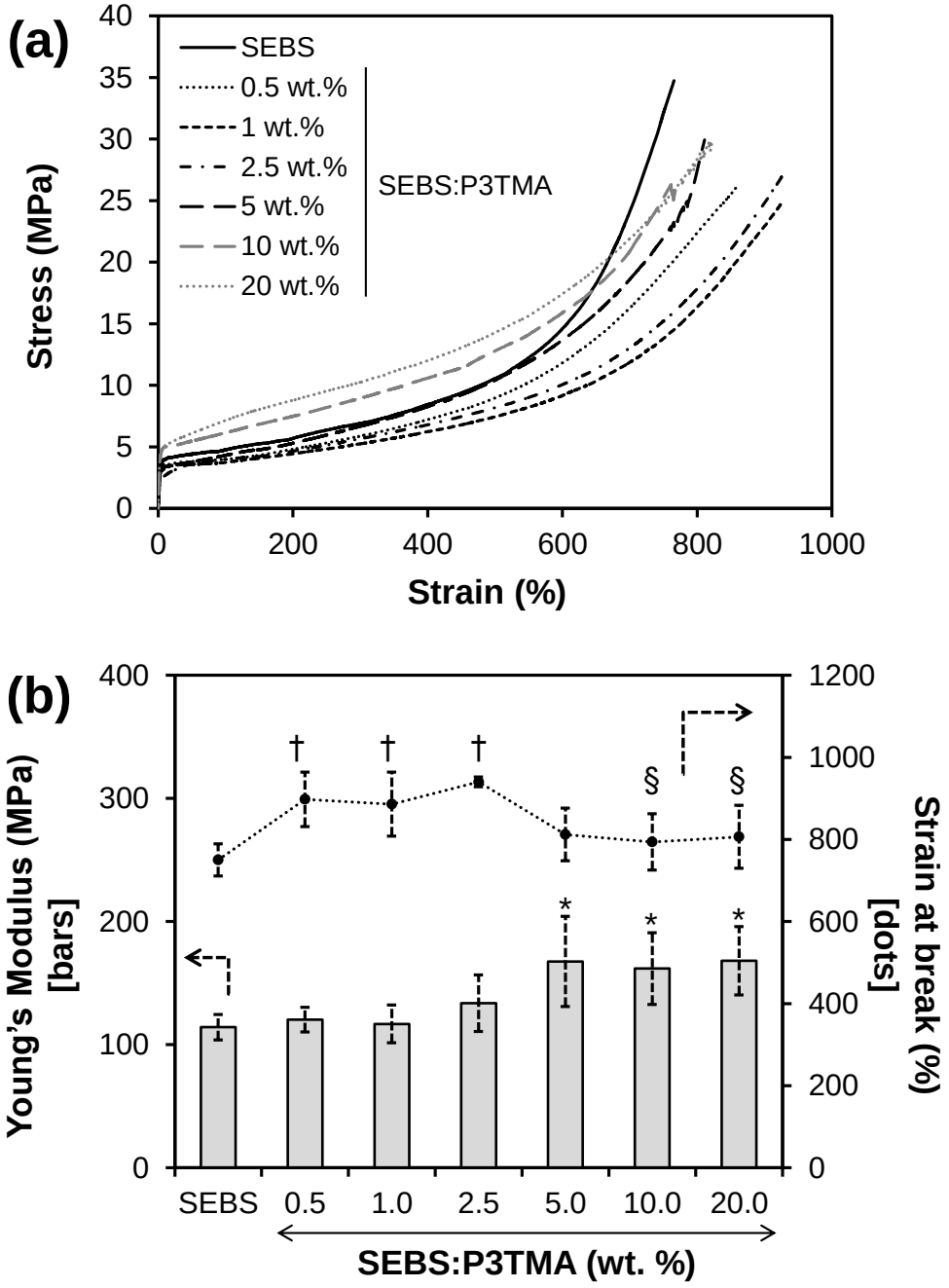

Figure 3. Mechanical properties for SEBS:P3TMA films: (a) Stress-strain curves; and (b) elastic modulus (bars, left axis) and strain at break values (dots, right axis). Tukey test ($p < 0.05$): * *vs.* (SEBS, 0.5 wt. % and 1 wt. %); † *vs.* SEBS and § *vs.* 2.5 wt. %.

This is the post-print (i.e. final draft post-refereeing) of the publication.
The final publication is available at Wiley Online Library via http://dx.doi.org/10.1002/polb.24095

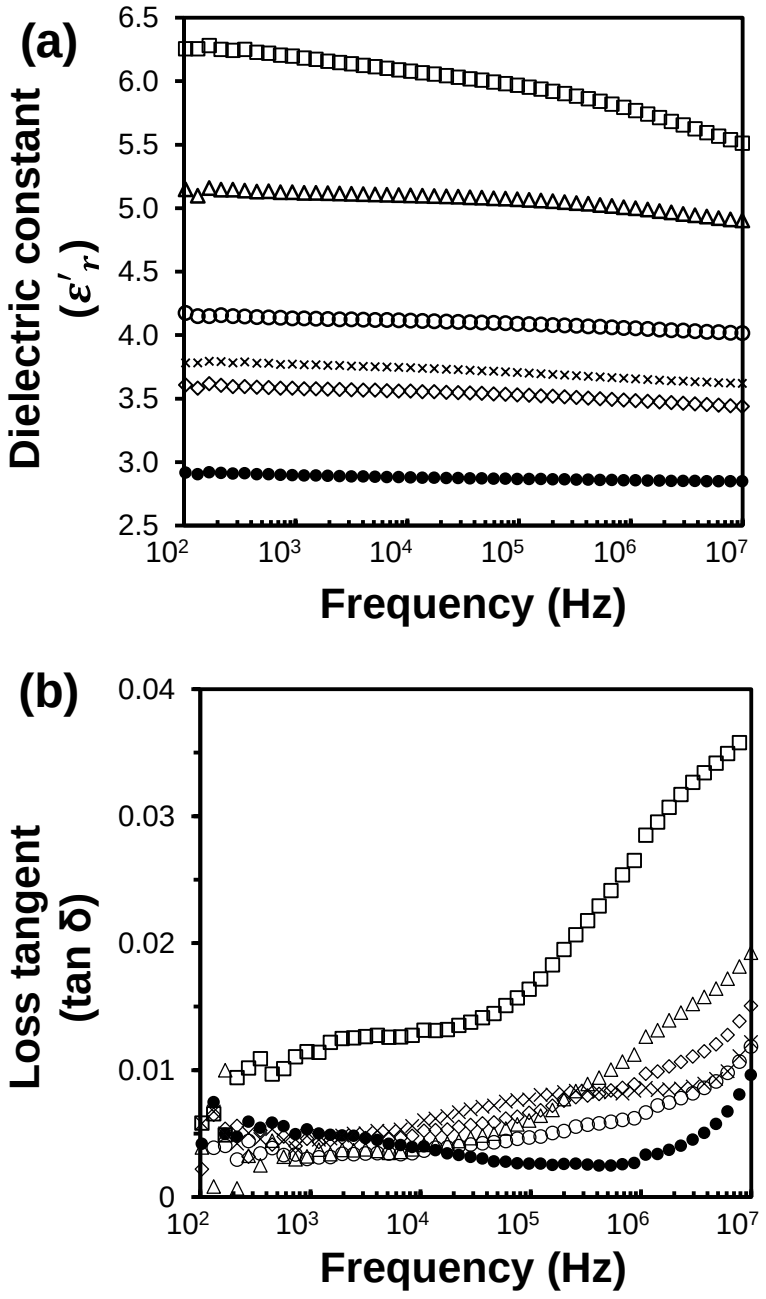

Figure 4. (a) Dielectric constant and (b) dielectric loss tangent as a function of frequency at room temperature (23 ºC) for SEBS (black circle) and SEBS:P3TMA films (empty symbols) containing 1 wt. % (diamond), 2.5 wt. % (circle), 5 wt. % (cross), 10 wt. % (triangle) and 20 wt. % (square) of P3TMA particles.

This is the post-print (i.e. final draft post-refereeing) of the publication.
The final publication is available at Wiley Online Library via http://dx.doi.org/10.1002/polb.24095

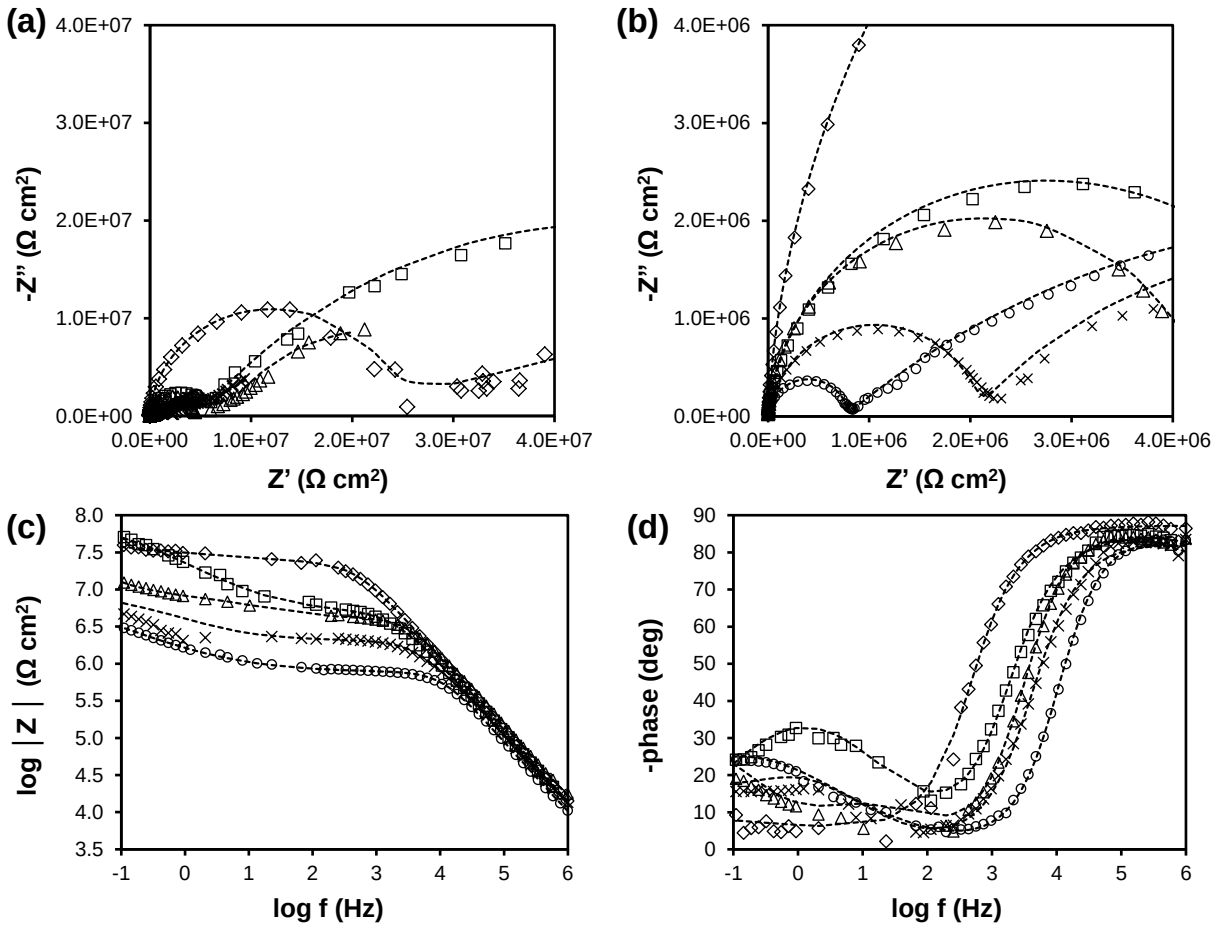

Figure 5. (a-b) Nyquist and (c-d) Bode plots for SEBS (diamond) and SEBS:P3TMA films containing 0.5 (square), 5 (triangle), 10 (cross) and 20 (circle) wt. % P3TMA. Symbols correspond to experimental data, while lines are fitted curves.